Effect of the Reynolds number on three- and four-particle diffusion in three-dimensional turbulence using kinematic simulation

F. Nicolleau*
The University of Sheffield, Department of Mechanical Engineering, Mapping Street, Sheffield, S1 3JD, United Kingdom

A. ElMaihy
Department of Mechanical Power and Energy, Military Technical College, Cairo, Egypt

(Received 11 July 2006; published 9 October 2006)

We study the evolution of three- and four-particle diffusion at large Reynolds numbers using kinematic simulation (KS) in isotropic turbulent flows. We vary the Reynolds number and find that the geometrical characteristics of triangles and tetrahedrons as functions of time do not depend on the Reynolds number but only on the ratio Δ_0/L_1 that is on the portion of the inertial range that was contained within the triangle or tetrahedron at the initial time. We also study the effect of the modeling of the unsteadiness term in the KS.

DOI: 10.1103/PhysRevE.74.046302 PACS number(s): 47.27.tb, 47.27.E−

I. INTRODUCTION

Turbulent mixing has a wide range of applications from the prediction of combustion in stroke engine to that of dispersion of pollutants in geophysical flows. It is also of fundamental importance for the study of turbulence. Batchelor [1] addressed the link between the statistics of the fluid motion and that of the passive scalar transport in turbulent flows. The statistical properties of scalar fluctuations have many similarities with the statistics of the turbulent velocity itself [2]. The traditional study of the correlation at two points is not sufficient to relate the scaling and the spatial structures of the flow field. Mydlarski [3] stressed the importance of the Lagrangian evolution of n particles in the study of the structure function of order n which is considered as a way to connect the scaling properties of a turbulent field and the spatial structure of the flow.

One- and two-particle studies involve simple statistics: the mean square displacement in the case of one-particle diffusion and the mean square separation between the two particles in the case of two-particle diffusion, whereas the multiparticle evolution exhibits nontrivial statistical conservation laws that involve geometry and power law for the increase of particles' separation. The distance growth is balanced by the decrease of shape fluctuation [4]. The existence of multiparticle conservation laws indicates the existence of long time memory effects and is a reflection of the coupling among the particles due to their presence in the same flow.

The statistics of the geometry of Lagrangian trajectories of three- and four-particle objects was investigated in three-dimensional turbulent flows using direct numerical simulation (DNS) [5] at a moderate Reynolds number ($R_\lambda=82$) which corresponds to a ratio of inertial scales $k_N/k_1=185$. The DNS demonstrated that initially regular clusters of points whose sizes lie in the dissipation range are strongly distorted, while clusters whose sizes are comparable to the integral length scale relax towards a uniform shape distribution. Because of the Reynolds number limitations when using DNS, Pumir *et al.* [5] used a phenomenological model of Lagrangian kinematics [6] which describes the combined action of coherent and incoherent random strains. The phenomenological model allowed them to qualitatively extrapolate the DNS results to larger Reynolds number regimes.

Castiglione and Pumir [7] studied the evolution of a three-particle swarm by tracking three points in an experimental turbulent two-dimensional flow with an inverse energy cascade regime with a $k^{-5/3}$ spectrum. The distribution of the triangle's shape was found to depend on its size. When the triangle size R is in the inertial range and grows according to $t^{3/2}$, a self-similar, non-Gaussian probability distribution is observed. When the triangle size is larger than the integral length scale, the shape distribution is Gaussian. But here again the experiment was done for a very small Reynolds number $k_N/k_1=3.76$ and the results obtained, discussed, and compared with the prediction of the phenomenological model introduced in Ref. [5].

In this paper we propose to use kinematic simulation (KS) to extend the previous results to larger Reynolds numbers. KS is a Lagrangian model of turbulent diffusion that is described in Sec. III. It is a model and needs first to be assessed against present data. This is done in Sec. IV A for three particles and in Sec. V A for four particles.

KS results already agree with the experimental results concerning two-particle statistics [8], concentration variance [9], and with DNS of two-particle dispersion [10]. KS is simple and less time consuming than a DNS or a large Eddy simulation (LES), and large Reynolds numbers can be achieved. It can therefore be used to test many cases to study the effect of the Reynolds number and the initial separation on the statistics of the dispersion of n particles. It has been successfully validated on the prediction of the fractal dimension of a line which is indeed a n-particle problem [11].

Khan *et al.* [12] also used KS to study the evolution of triangles in two-dimensional turbulent flows. They used KS to reproduce the experiment in Ref. [7] and studied the effect of high inertial ranges $k_N/k_1=1$, 691, 3381, and 16 909. They concluded that as the Reynolds number is increased the variables describing the geometry, $\langle I_2\rangle$, $\langle w\rangle$, and $\langle \chi\rangle$, become weaker functions of both the triangle's initial size and time.

*Electronic address: F.Nicolleau@Sheffield.ac.uk

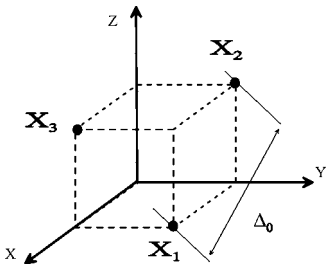

FIG. 1. Initial positions of a cluster of three particles.

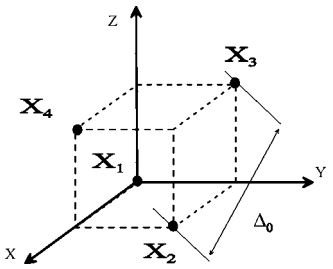

FIG. 2. The initial positions of a cluster of four particles

The values of these variables were always found significantly different from the Gaussian values.

In this paper, we study the effect of the Reynolds number, initial size, and unsteadiness term modeling in three-dimensional flows for triangles in Sec. IV and for tetrahedron in Sec. V. Conclusions are summarized in Sec. VI.

II. MULTIPARTICLE PARAMETRIZATION

In this section we introduce the parameters used to evaluate the dispersion of three and four particles.

A. Three-particle parametrization

We start with three particles located at $\mathbf{X}_i$ $(i=1,3)$, as shown in Fig. 1. The initial positions of the particles are chosen randomly in each realization such that the initial separation between any two particles is set to a given value Δ_0. To enhance randomness in the different realizations, the cube shown in Fig. 1 is rotated by a random angle for each realization.

To describe the evolution of the size and shape of the three-particle cluster corresponding to the points $\mathbf{X}_1$, $\mathbf{X}_2$, and $\mathbf{X}_3$ we use the parametrizations introduced in Refs. [6,13] for our analysis.

The two reduced vectors ρ_i, independent of the center of mass variable ρ_0 are defined as follows:

$$\rho_1 = \frac{\mathbf{X}_2 - \mathbf{X}_1}{\sqrt{2}}, \quad \rho_2 = \frac{2\mathbf{X}_3 - \mathbf{X}_1 - \mathbf{X}_2}{\sqrt{6}}. \tag{1}$$

The radius of gyration is then defined as

$$R^2 = {\rho_1}^2 + {\rho_2}^2 = \frac{r_{12}^2 + r_{23}^2 + r_{31}^2}{3}, \tag{2}$$

where the $r_{ij}=|\mathbf{X}_j-\mathbf{X}_i|$ are the length of the triangle sides. It is used to define the characteristic size of the triangle. The area of the triangle is defined as

$$A = |\rho_1 \times \rho_2|. \tag{3}$$

In order to characterize the shape of the triangle, Pumir *et al.* [5] introduce a "moment of inertia-like" tensor $\mathbf{g}^{ab}$ as follows:

$$\mathbf{g}^{ab} = \sum_{i=1}^{2} \rho_i^a \rho_i^b, \tag{4}$$

where ρ_i^a is the a component of the vector ρ_i. This tensor has three eigenvalues g_1, g_2, and g_3 that describe the spatial extension of the triangle $(\mathbf{X}_1, \mathbf{X}_2, \mathbf{X}_3)$ in the three-dimensional turbulence. The triangle continuously experiences dilatation, rotation, and translation during its evolution in the turbulent flow, so its size and shape are varying continuously. One method to quantify the shape of the triangle is to monitor the quantity I_2 which is defined as the ratio between g_2 the smallest eigenvalue and R^2,

$$I_2 = \frac{g_2}{R^2}. \tag{5}$$

I_2 varies between 0 and 1/2, an equilateral triangle corresponds to a value of $I_2=1/2$, smaller values of I_2 correspond to more elongated triangles.

Another method to describe the shape of the triangle is to use the parameters w and χ [7] which are defined as

$$w = 2\frac{|\rho_1 \times \rho_2|}{R^2} \tag{6}$$

so that $w \in [0,1]$, and

$$\chi = \frac{1}{2}\arctan\left[\frac{2\rho_1 \cdot \rho_2}{{\rho_2}^2 - {\rho_1}^2}\right]. \tag{7}$$

Because of the global invariance of the triangles under any relabeling of the three vertices, it can be shown that $\chi \in [0, \pi/6]$ [13]. The ratio I_2 defined previously is related to w as follows:

$$I_2 = (1 - \sqrt{1 - w^2})/2. \tag{8}$$

The value $w=0$ indicates that the three points are aligned, whereas the value $w=1$ corresponds to an equilateral triangle. Small values of χ indicate that the separation between any two particles (e.g., 1 and 2) is much smaller than their separation with the third one. (See Fig. 3 in Ref. [14].)

B. Four-particle parametrization

The initial position of the four-particle cluster corresponds to the points $\mathbf{X}_1$, $\mathbf{X}_2$, $\mathbf{X}_3$ and $\mathbf{X}_4$ as shown in Fig. 2. For a four-particle cluster in addition to ρ_1 and ρ_2 we have to define ρ_3 as follows:

$$\rho_3 = \frac{3\mathbf{X}_4 - \mathbf{X}_1 - \mathbf{X}_2 - \mathbf{X}_3}{\sqrt{12}}. \tag{9}$$

The radius of gyration which is defined as $R^2=\Sigma_{i=1}^3 {\rho_i}^2$ is used to measure the size of the four-particle cluster. To character-

ize the shape of the object Pumir *et al.* [5] generalized the "moment of inertia-like" tensor to

$$\mathbf{g}^{ab} = \sum_{i=1}^{3} \rho_i^a \rho_i^b. \tag{10}$$

The eigenvalues of this tensor g_i $(i=1,2,3,4)$ provide a way of quantifying the shape of the set of points. $g_1=g_2=g_3$ corresponds to an isotropic object. The case $g_1 \approx g_2 \gg g_3$ corresponds to a pancakelike object and $g1 \gg g_2$, g_3 to a needlelike object.

The dimensionless parameter I_2, defined by $I_2=g_2/R_2$, is used to describe the overall shape of the tetrahedron. The volume of the tetrahedron defined as

$$V = |\det(\rho_1, \rho_2, \rho_3)| \tag{11}$$

can also be used to characterize the evolution with time.

III. KINEMATIC SIMULATION

A. Introduction to kinematic simulation

The n-particle dispersion is modeled using kinematic simulation (KS). Kinematic simulation is now a well-established Lagrangian model. In contrast to classical stochastic models, it is the Eulerian velocity field which is modelled by kinematic simulation and it generates realistic particle trajectories. In that sense a detail modeling of turbulence features is not always necessary. Furthermore, from a theoretical point of view it is paramount to understand what is necessary and what is not for a correct geometrical description of the turbulence. The pseudo-Eulerian velocity field, $\mathbf{u}_{KS}(\mathbf{x},t)$, is usually expressed as a finite and discrete sum of Fourier modes [15]:

$$\mathbf{u}_{KS}(\mathbf{x},t) = \sum_{n,m} \mathbf{A}_{nm} e^{\mathbf{k}\dot{\mathbf{x}}+\omega t},$$

where $\mathbf{x}$ is the position of the fluid particle. In practice, kinematic simulation then relies on the integration of

$$\frac{d\mathbf{x}}{dt} = \mathbf{u}_{KS}(\mathbf{x},t), \tag{12}$$

geometrical features and other constraints (incompressibility) are introduced as constraints on the coefficients of the decomposition $\mathbf{A}_{nm}$, and the energy spectrum is prescribed according to the type of turbulence considered.

Many researches [9,10,16,17] suggest that from rather crude information from the Eulerian velocity field, KSs reproduce many relevant geometrical features of Lagrangian turbulence that have significant qualitative and quantitative implications on concentration fields. Comparisons of direct numerical simulation results for two-particle statistics in stationary isotropic turbulence have shown good agreement with KS [8–10,18]. It was found that KS models reproduce well the global statistical properties of Lagrangian intermittency at the Reynolds numbers attainable by DNS. In KS, as in DNS and real turbulent flows, the non-Markovian geometry of trajectories is determined by the eddying, straining, and perhaps also other structures in individual Eulerian realizations. Such structures are not implemented in random walks or Reynolds average Navier-Stokes equation (RANS), and their fine detail may not matter for some Lagrangian statistics. However, the presence of these sort of structures is pivotal and can explain various Lagrangian properties such as aspects of two-particle dispersion, power spectra, etc.

As in Refs. [11,19] our three-dimensional (3D) KS velocity field is given as a sum of N random Fourier modes, i.e.,

$$\mathbf{u}(\mathbf{x},t) = \sum_{n=1}^{N} (\mathbf{a_n} \times \hat{\mathbf{k}}_n)\cos(\mathbf{k}_n \cdot \mathbf{x} + \omega_n t) + (\mathbf{b_n} \times \hat{\mathbf{k}}_n)\sin(\mathbf{k}_n \cdot \mathbf{x} + \omega_n t).$$

$\hat{\mathbf{k}}_n$ defined as $\hat{\mathbf{k}}_n = \mathbf{k}_n/|\mathbf{k}_n|$ is a random unit vector. $\mathbf{a}_n$ and $\mathbf{b}_n$ are random and uncorrelated vectors with their amplitudes being chosen according to a prescribed power law energy spectrum $E(k)$, i.e.,

$$|\mathbf{a}_n \times \hat{\mathbf{k}}_n|^2 = |\mathbf{b}_n \times \hat{\mathbf{k}}_n|^2 = 2E(k_n)\Delta k_n \tag{13}$$

and

$$\left.\begin{aligned} E(k) &= \frac{u_0^2}{k_1}\left(\frac{k}{k_1}\right)^{-5/3} \quad \text{for } k_1 \leqslant k \leqslant k_N \\ E(k) &= 0 \qquad\qquad\quad \text{otherwise} \end{aligned}\right\}. \tag{14}$$

B. Kinematic simulation's parameters

Typical turbulence parameters we define are the integral length scale

$$L = \frac{3\pi}{4}\frac{\int_{k_1}^{k_N} E(k)k^{-1}dk}{\int_{k_1}^{k_N} E(k)dk}. \tag{15}$$

We also introduce $L_1=2\pi/k_1$, the largest scale of the inertial range, the turbulent velocity fluctuation intensity,

$$u' = \sqrt{\frac{2}{3}\int E(k)dk},$$

and the Kolmogorov length scale, defined here as

$$\eta = \frac{2\pi}{k_N},$$

the characteristic time associated to this scale is

$$\tau_\eta = \frac{L}{u'}\left(\frac{\eta}{L}\right)^{2/3}.$$

The distribution of the wave number is geometric, i.e.,

$$k_n = k_1\left(\frac{k_N}{k_1}\right)^{(n-1)/(N-1)}. \tag{16}$$

It is also possible to introduce a frequency ω_n that determines the unsteadiness associated with the nth wave mode. Here,

the value of the unsteadiness coefficient λ is defined by two methods.

Method 1. We follow Malik and Vassilicos [10] who chose ω_n to be proportional to the eddy-turnover time of the nth wave mode, i.e.,

$$\omega_n = \lambda \sqrt{k_n^3 E(k)}, \tag{17}$$

where λ is the unsteadiness parameter and may be expected to be of the order of 1. It has been shown in 3D isotropic KS [10] that for two-particle diffusion most statistical properties are insensitive to the unsteadiness parameter's value provided that it rests in the range $0 \leqslant \lambda \leqslant 1$. Nicolleau and El-Maihy [11] also concluded that, in that range of values, λ has no effect on the fractal dimension of a cloud of fluid particles.

Method 2. For the sake of completeness we also use a second method were ω_n is chosen as a random variable uniformly distributed in the range

$$\omega_n \in [-\lambda \sqrt{k_n^3 E(k)}, \lambda \sqrt{k_n^3 E(k)}]. \tag{18}$$

For the sake of simplicity we set the initial time when the particles are released to 0.

C. Initial positions

The initial position of the first particle is chosen randomly in each realization, then the initial positions of the other particles are calculated relative to the first particle such that the initial separation between any two particles is set to $\Delta_0 = q\eta$ where $q = 1/4$, 1, 4, 16, 32, and 64 as shown in Fig. 1 for three particles and Fig. 2 for four particles.

We follow the evolution with time of the n-particle object, which is initially isotropic, by solving Eq. (12) for each particle using the fourth order predictor corrector method (Adams-Bashforth-Moulton) in which Runge Kutta 4 is used to compute the first three points in Adams-Bashforth method. Other schemes have been investigated for sake of comparison, the Adams-Bashforth-Moulton scheme gave the best performance in terms of error growth, stability, and computing time. The parameters V, I_2, w, and χ are calculated at each time step and then averaged over 4000 realizations.

The computation is made first for small Reynolds numbers to allow us to compare our results with the results obtained experimentally in Ref. [7] and using DNS in Ref. [5].

Then the evolution of three and four particles is made for larger Reynolds numbers to study the effect of different inertial subranges. The value of the unsteadiness coefficient λ defined by methods 1 and 2 is varied to study the effect of the unsteadiness parameter on three- and four-particle diffusion. Table I shows the different simulation parameters used to predict three- and four-particle diffusion.

IV. THREE-PARTICLE RESULTS

We are interested in the evolution of the size and geometry of an initially equilateral triangle. The evolution of the triangle's size is obtained by computing the evolution of $\langle R^2 \rangle^{1/2}$ as a function of time for different initial sizes Δ_0. The alteration of the triangle's shape can be observed by computing the evolution of $\langle I_2 \rangle$, $\langle w \rangle$, and $\langle \chi \rangle$ as functions of time.

TABLE I. Different simulation parameters used to predict three- and four-particle diffusion using KS. Other constant parameters are $u' = 1$ and $L/u' = 1$.

k_N/k_1	t_η	η	Δ_0/η	λ
185	0.031	0.03398	0.25, 1, 4, 5.92,	0
			16, 32, 64, 92.5	0
1000	0.01	0.006286	0.25, 32, 500	0
1000	0.01	0.006286	0.25	1
1000	0.01	0.006286	0.25	5
1000	0.01	0.006286	0.25	20
2000	0.0063	0.003143	0.25, 1, 4, 32, 64, 1000	0

A. Validation

The computations are first made for a small inertial subrange ($k_N/k_1 = 185$) to allow the validation of our results against the DNS results of Ref. [5] and the experimental work of Ref. [7], then another set of computations is made for $k_N/k_1 = 2000$ to study the effect of large Reynolds numbers on the diffusion of three-particle clusters.

Figure 3 shows the evolution of the triangle's average size $\langle R^2 \rangle^{1/2}$ as a function of time for different initial sizes, namely $\Delta_0 = 0.25\eta$, η, 4η, 16η, 32η, 64η, and 92.5η. The slope 3/2 corresponds to the estimation of the Richardson regime, whereas the slope 1/2 indicates the large time random walk regime. As expected from definition (2), the figure shows the same characteristic regimes as for two-particle separation, in particular there is no clear Richardson regime in this type of representation except for $\Delta_0 \sim \eta$ (see Ref. [19] for a discussion on the nature of the Richardson regime).

Because of the finite size of the experiment cell, the increase of the radius of gyration saturates to a certain value in an experiment [7], whereas, in our three-dimensional KS, $\langle R^2 \rangle$ increases with t up to very long times ($tu'/L > 10$) as

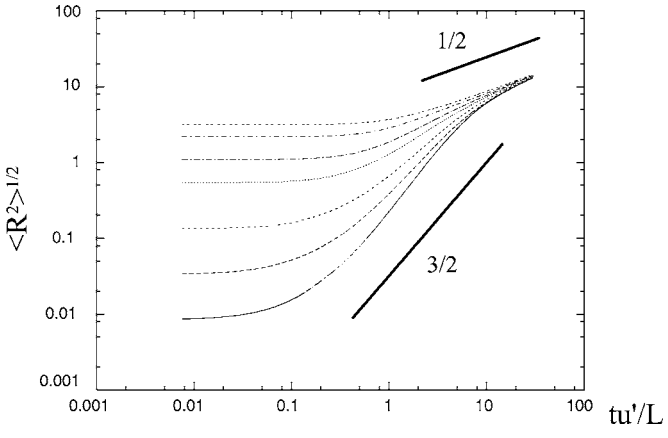

FIG. 3. Time evolution of the triangle size for $k_N/k_1 = 185$ and different triangle initial sizes from bottom to top $\Delta_0/\eta = 0.25$, 1, 4, 16, 32, 64, and 92.5.

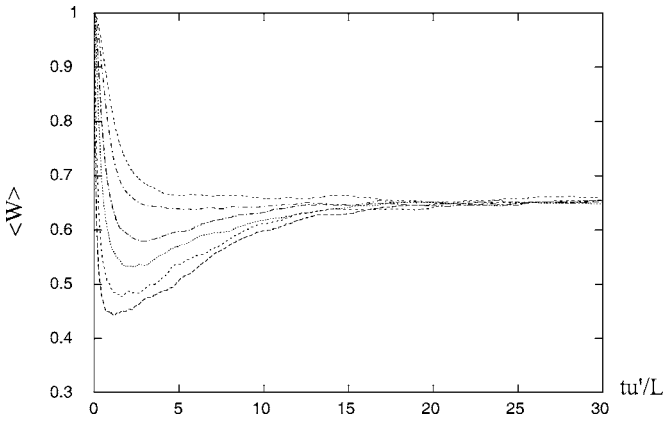

FIG. 4. Time evolution of $\langle w \rangle$ for $k_N/k_1=185$ and different triangle initial sizes from bottom to top: $\Delta_0/\eta=0.25$, 1, 4, 16, 32, 64, and 92.5.

shown by the line with a 1/2 slope in Fig. 3. Khan *et al.* noticed the same behavior in a two-dimensional KS.

The evolutions of $\langle w \rangle$ and $\langle I_2 \rangle$ as functions of the normalized time tu'/L for different initial sizes Δ_0/η are shown respectively in Figs. 4 and 5. The evolution of $\langle \chi \rangle$ for the same cases is shown in Fig. 6. Where $0<\Delta_0 \ll 0.5L_1$, all these quantities decrease rapidly owing to the strong shape distortion of the triangle towards a minimum value. This minimum value is an increasing function of the initial size. The maximum shape distortion is observed for $\Delta_0/\eta=0.25$ at $tu'/L \simeq 2$. When the initial triangle size becomes comparable to the largest length scale L_1 ($\Delta_0 \simeq 0.5L_1$), we find that $\langle w \rangle$, $\langle I_2 \rangle$, and $\langle \chi \rangle$ decrease directly from their initial values to their asymptotic values without passing through a minimum value.

At large times $tu'/L>15$ the three points eventually lose memory of their initial separations and all curves for all initial sizes approach the same asymptotic value, which is 0.66 for $\langle w \rangle$, 0.16 for $\langle I_2 \rangle$, and 0.26 for $\langle \chi \rangle$. This value of $\langle I_2 \rangle_{asy}$ corresponds to a Gaussian distribution of ρ_1 and ρ_2 which leads to a Gaussian distribution of $\langle I_2 \rangle$. For three-dimensional turbulent flows $\langle I_2 \rangle_{Gau}=1/6$ [5].

The time at which the distributions of the shape parameter relax to the asymptotic value is shown to be dependent on the initial triangle size. At a given initial triangle size, if one

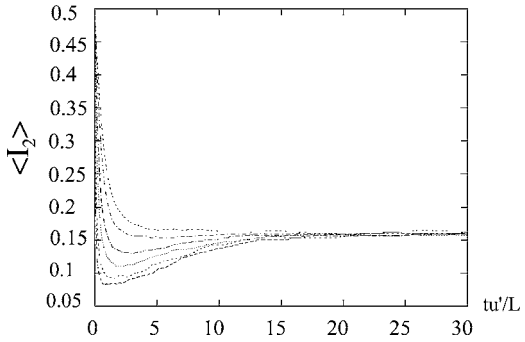

FIG. 5. Time evolution of $\langle I_2 \rangle$ for $k_N/k_1=185$ and different triangle initial sizes from bottom to top: $\Delta_0/\eta=0.25$, 1, 4, 16, 32, 64, and 92.5.

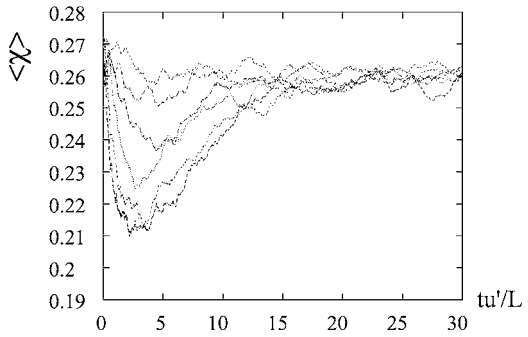

FIG. 6. Time evolution of $\langle \chi \rangle$ for $k_N/k_1=185$ and different triangle initial sizes $\Delta_0/\eta=0.25$, 1, 4, 16, 32, 64, and 92.5.

of the particles disperses faster than the others, the triangle is elongated and the time needed for the triangle to have a uniform distribution depends on how the other particles will separate. The two particles with initially small separation will stay together for a longer time until separation takes place and as a result the time needed for the triangle to have a uniform distribution increases.

From these results, KSs are found to satisfactorily predict the evolution of three-particle diffusion in homogeneous isotropic three-dimensional turbulent flows. The results are in full agreement with DNS results in Ref. [5] for three-dimensional turbulence and experimental results for two-dimensional turbulence [7].

B. Larger inertial ranges

We now consider larger inertial ranges (k_N/k_1) to investigate how the size and shape of a three-particle cluster evolve at higher Reynolds numbers. Computations are done for different inertial ranges k_N/k_1, namely 185, 1000, and 2000 and for different initial triangle sizes.

Figure 7 shows the evolution of $\langle w \rangle$ as a function of tu'/L for $k_N/k_1=2000$ and different triangle initial sizes $\Delta_0/\eta=0.25$, 1, 4, 32, 64, and 1000. If we compare the results with those for $k_N/k_1=185$ in Fig. 4, it looks as if $\langle w \rangle$ depended on both Δ_0/η and k_N/k_1. By contrast, Fig. 8 shows the same

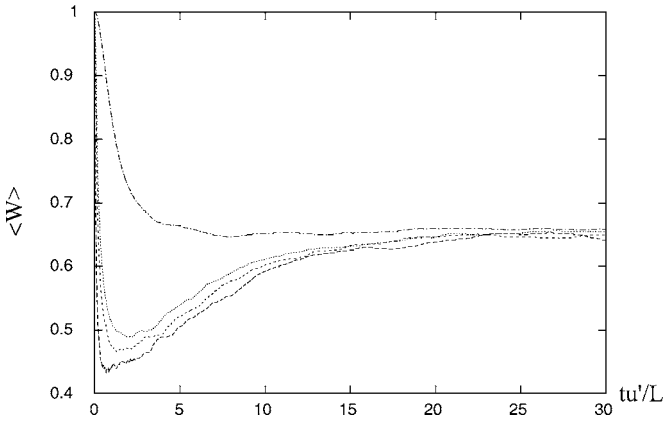

FIG. 7. Time evolution of $\langle w \rangle$ for $k_N/k_1=2000$ and different triangle initial sizes from bottom to top $\Delta_0/\eta=0.25$, 1, 4, 32, 64, and 1000.

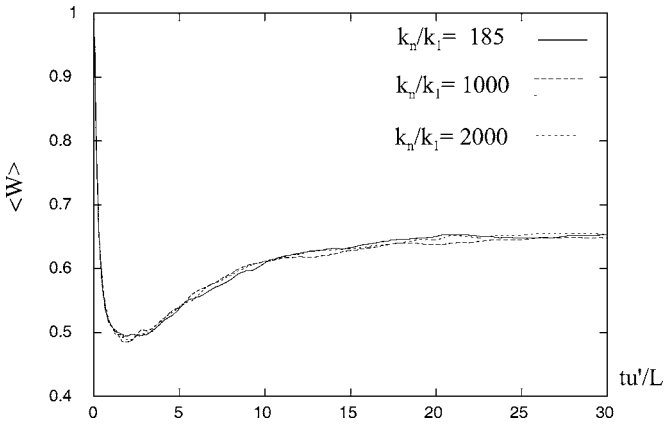

FIG. 8. Time evolution of $\langle w \rangle$ for different inertial subranges $k_N/k_1=185$, 1000, and 2000, and $\Delta_0/L_1=0.032$.

evolution of $\langle w \rangle$ but this time for different inertial subranges $k_N/k_1=185$, 1000, and 2000, and a given Δ_0/L_1. In this case $\langle w \rangle$ is independent of k_N/k_1. This result was observed for all ratio Δ_0/L_1, so in fact $\langle w \rangle$ is not a function of k_N/k_1 but a function of Δ_0/L_1:

$$\langle w \rangle = \mathcal{F}_w(\Delta_0/L_1, tu'/L). \tag{19}$$

Or, provided that Δ_0/L_1 is kept constant, $\langle w \rangle$ as a function of tu'/L does not depend on k_N/k_1 that is on the Reynolds number.

The same result is shown in Figs. 9 and 10 for $\langle \chi \rangle$:

$$\langle \chi \rangle = \mathcal{F}_\chi(\Delta_0/L_1, tu'/L) \tag{20}$$

does not depend on k_N/k_1 and for $\langle I_2 \rangle$ in Figs. 11 and 12:

$$\langle I_2 \rangle = \mathcal{F}_I(\Delta_0/L_1, tu'/L) \tag{21}$$

is also independent of k_N/k_1.

Pumir *et al.* [5] concluded that their results did not depend qualitatively on the Reynolds number in the range $21 < R_\lambda < 82$. We can extend this range to the higher limit $k_N/k_1 = 2000$ which corresponds to $R_\lambda = 400$. These results are to be

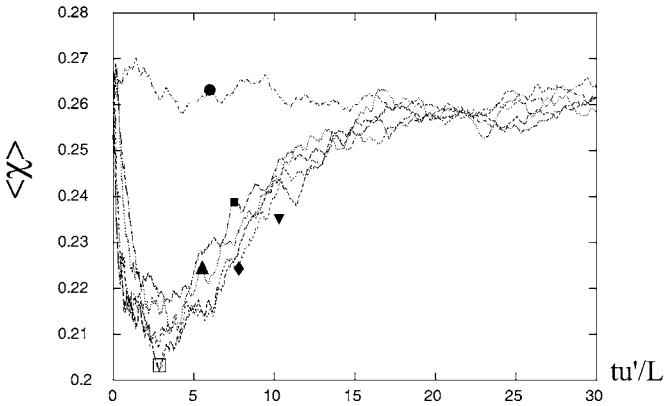

FIG. 9. Time evolution of $\langle \chi \rangle$ for $k_N/k_1=2000$ and different triangle initial sizes $\Delta_0/\eta=0.25$ (▼), 1 (□), 4 (♦), 32 (▲), 64 (■), and 1000 (●).

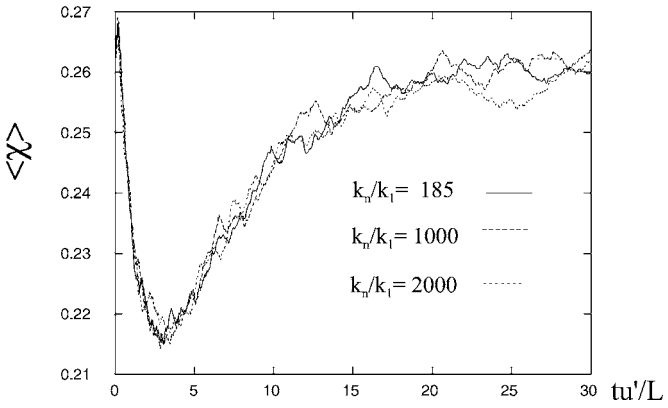

FIG. 10. Time evolution of $\langle \chi \rangle$ for different inertial subranges $k_N/k_1=185$, 1000, and 2000, and $\Delta_0/L_1=0.032$.

related to the findings of Ref. [11]. In this paper, similar results were found for the fractal dimension of a volume evolving in a turbulent flow, namely that

$$D_v = 3 - C\frac{L}{\Delta_0}\left(\frac{tu'}{L}\right)^{1/3}, \tag{22}$$

where D_v is the fractal dimension of what was initially a volume, Δ_0 is its initial characteristic scale, and C a constant. Equation (22) also is independent of the ratio k_N/k_1, that is of the Reynolds number, but is a function of Δ_0/L. What matters in the building up of the fractal dimension is the scales present inside the volume that is the ratio L/Δ_0. Here, we can reach the same conclusion for I_2, w, and χ, their evolution is controlled by L/Δ_0 that is the range of turbulent scales the initial triangle encompasses and not by the inertial range ratio k_N/k_1.

Figures 7, 12, and 9 show the evolution of $\langle w \rangle$, $\langle I_2 \rangle$, and $\langle \chi \rangle$ as functions of tu'/L for $k_N/k_1=2000$ for different initial triangle sizes Δ_0, namely $\Delta_0/\eta=0.25$, 1, 4, 32, 64, and 1000. The dependence of these parameters on the initial triangles sizes is shown to be weaker than that for small Reynolds numbers. That is not in contradiction with the previous state-

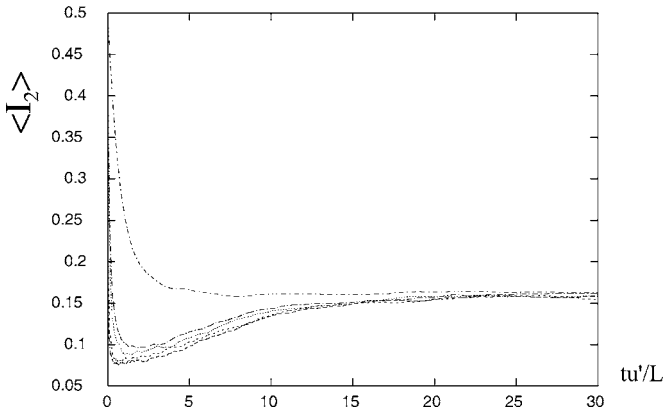

FIG. 11. Time evolution of $\langle I_2 \rangle$ $k_N/k_1=2000$ and different triangle initial sizes, from bottom to top $\Delta_0/L_1=0.032$, 1, 4, 32, 64, 1000.

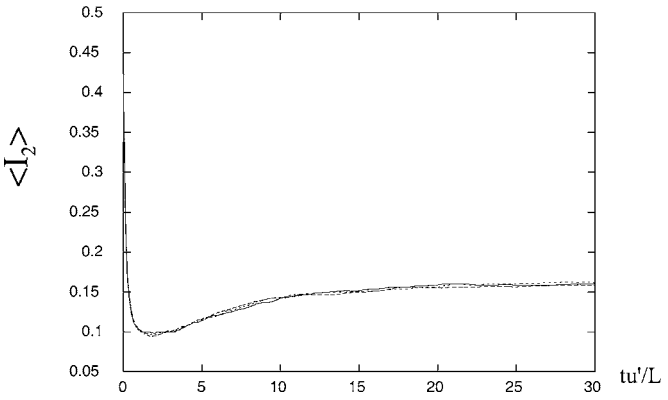

FIG. 12. Time evolution of $\langle I_2 \rangle$ for different inertial subranges $k_N/k_1=185$, 1000, and 2000 and $\Delta_0/L_1=0.032$.

ment that they are independent of k_N/k_1. In our KS, k_1 is fixed so increasing k_N/k_1 means increasing k_N as

$$\frac{\Delta_0}{L} \simeq \frac{\Delta_0}{\eta}\frac{k_1}{k_N},$$

comparing cases where k_N/k_1 is increasing at constant Δ_0/η is actually comparing cases where Δ_0/L is decreasing.

In contrast, with KS results for two-dimensional turbulent flows [12], all values of the parameters describing the triangle shape evolution approach an asymptotic value, which is the Gaussian value. Similarly to what is found at $k_N/k_1=185$, when the initial triangle size becomes comparable to the largest length scale L, $\Delta_0 \approx 0.5L_1$ (as can be seen in the case $\Delta_0=1000\eta$), we find that the parameters describing the shape's change decrease from their initial values to their final asymptotic values, directly, without decreasing to an intermediary minimum, as it is the case for smaller initial triangle sizes namely $\Delta_0 \ll 0.5L_1$. So, we can conclude that if the initial triangle size is in the inertial range but much larger than the Kolmogorov microscale, the shape distortion becomes very small. This would be because a triangle with an initial size large enough may not be affected by the small-scale fluctuations of the turbulent field. Such a triangle will contain all the scales of turbulence from the beginning so its evolution does not depend on Δ_0/L anymore.

C. Effect of the unsteadiness term on three-particle diffusion

Figure 13 shows the evolution of the triangle size $\langle R^2 \rangle^{1/2}$ as a function of tu'/L for $k_N/k_1=1000$, $\Delta_0/\eta=0.25$, and different unsteadiness parameters $\lambda=0$, 1, 5, and 20 defined by the first method (a) and the second method (b). It can be seen that provided that $0 \leqslant \lambda \leqslant 1$, there is no effect of λ on the evolution of the triangle size for times smaller than 7 tu'/L when using the first method, and at all times when using the second method.

The evolutions of the shape-based parameters $\langle I_2 \rangle$, $\langle w \rangle$, and $\langle \chi \rangle$ are shown in Figs. 14–16, respectively, for the same cases used in Fig. 13. When using the second method, varying λ for 0–20 affects $\langle I_2 \rangle$ and $\langle W \rangle$ by less than 10%. When using the first method, this is only true for $\lambda \in [0,1]$. With this method, larger values of λ change significantly $\langle I_2 \rangle$ and

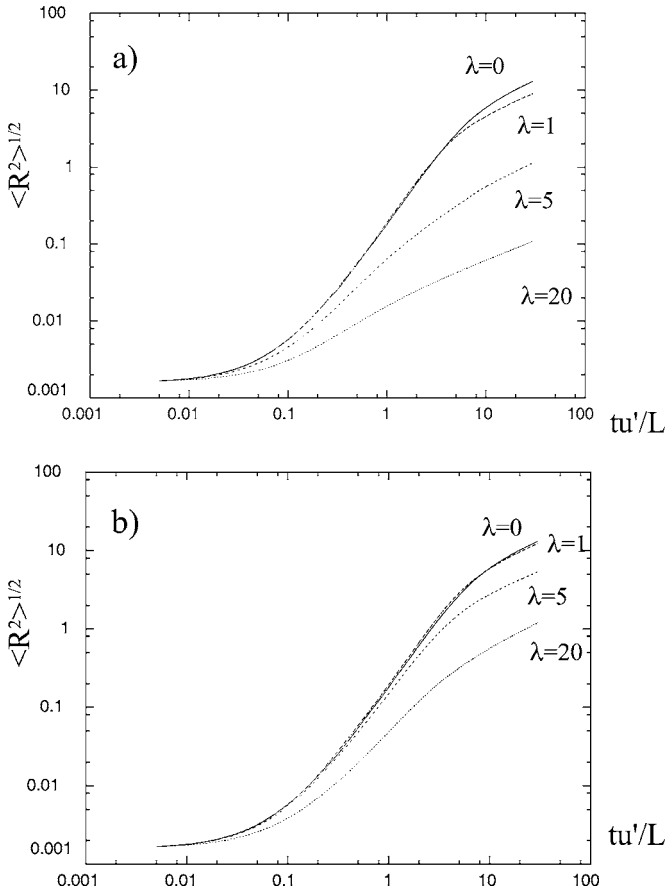

FIG. 13. Time evolution of the triangle size $\langle R^2 \rangle^{1/2}$ for $k_N/k_1=1000$, $\Delta_0/\eta=0.25$, and different unsteadiness parameters $\lambda=0$, 1, 5, and 20 defined by (a) the first method and (b) the second method.

$\langle w \rangle$ at times $t/u'L<10$. This mainly affects the time at which these two triangle shape parameters relax to their asymptotic values. This time is significantly decreased with the increase of λ when using the first method. This can be attributed to the following: as the value of λ increases the flapping of the velocity field increases, the particles decorrelate from each other more rapidly, and the triangle forgets its initial conditions faster. For $0 \leqslant \lambda \leqslant 1$ defined by either methods, the asymptotic value of $\langle I_2 \rangle$ is the same as the Gaussian value predicted at $\lambda=0$ but further increase λ (i.e., $\lambda>1$) will result in departures from the Gaussian value though by less than 10%.

As can be seen from Fig. 16, $\langle \chi \rangle$ is more sensitive to the value taken by λ, though here as well the second method is much more robust. Provided $\lambda \in [0,1]$ the error on the time at which the minimum is reached is again within 10% as is the error on the asymptotic value.

So we can conclude that the second method is rather robust and results are safe provided $\lambda \in [0,1]$. This result was already known for two-particle statistics, so studying three-particle objects does not add constraint on the modeling of the unsteadiness parameter.

D. Lagrangian autocorrelations for three particles

Figure 17 shows the Lagrangian autocorrelation function of the triangle's size R_c that is

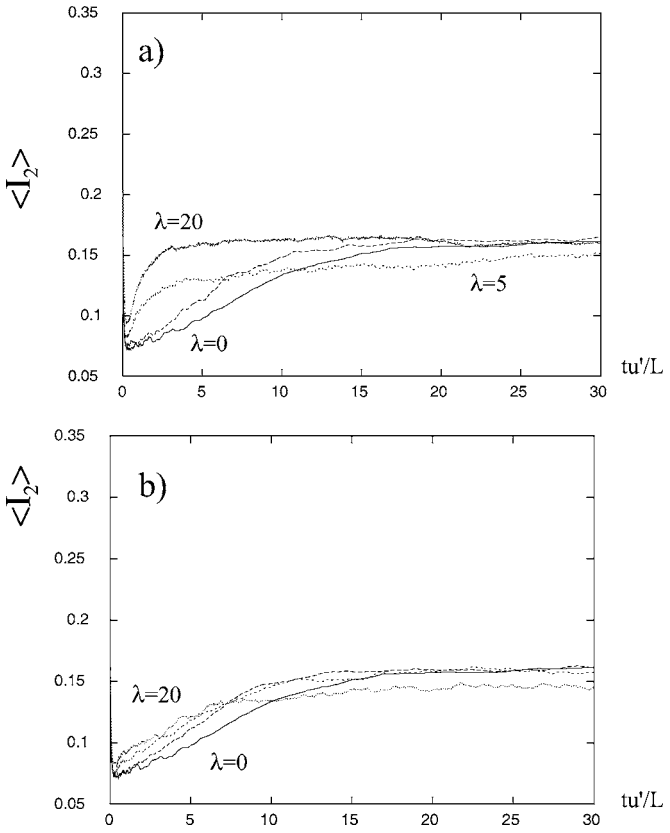

FIG. 14. Time evolution of $\langle I_2 \rangle$ for $k_N/k_1=1000$, $\Delta_0/\eta=0.25$, and different unsteadiness parameters $\lambda=0$, 1, 5, and 20 defined by (a) the first method and (b) the second method.

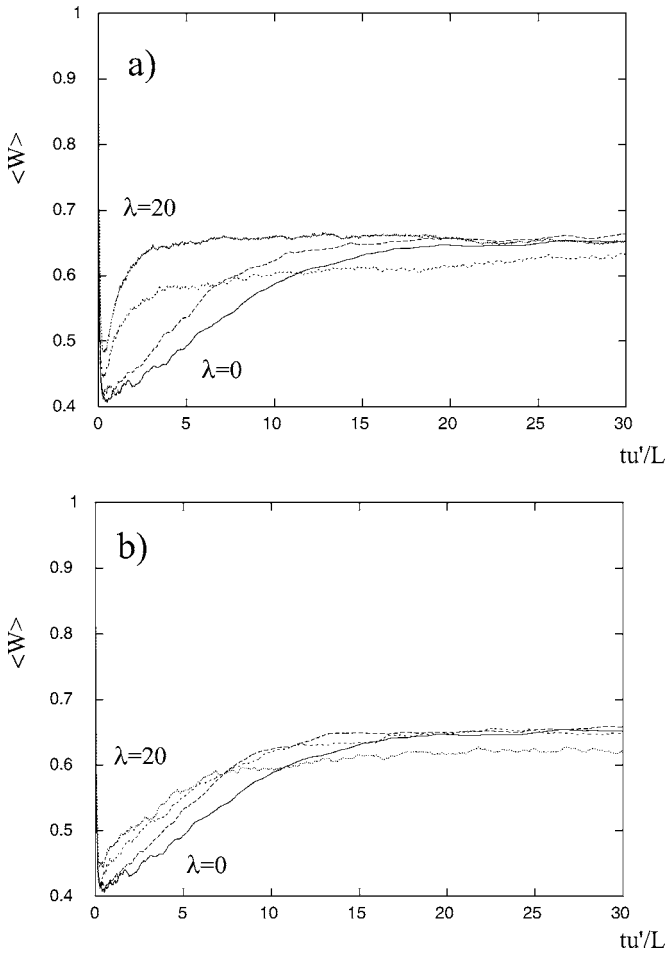

FIG. 15. Time evolution of $\langle w \rangle$ for $k_N/k_1=1000$, $\Delta_0/\eta=0.25$, and different unsteadiness parameters $\lambda=0$, 1, 5, and 20 defined by (a) the first method and (b) the second method.

$$R_c = \frac{\langle R(t,\tau)R(t,0)\rangle}{\langle R(t,0)^2\rangle}, \tag{23}$$

for different times in Richardson's range [20], namely $tu'/L=2.5$, 3, 3.5, 4, 4.5, and 5. All curves collapse indicating that the evolution of the radius of gyration is self-similar in time. The dashed straight line indicates that the radius of gyration remembers about 0.65 of its history. This value is larger than the value obtained for two-particle diffusion (0.56) indicating that for this parameter a three-particle cluster has a longer memory than a two-particle cluster. The self-similarity observed on the radius of gyration is much less obvious on the autocorrelation function of the parameter $\langle w \rangle$. As shown in Fig. 18, the correlation increases with tu'/L, the triangle remembers more of its previous shape when tu'/L increases as indicated by the the two dashed straight lines corresponding respectively to $tu'/L=2.5$ and 5.

V. FOUR-PARTICLE RESULTS

A. Comparison with low Reynolds number DNS

In this section, we follow the tetrahedron of Fig. 2. We are interested in the evolution of the tetrahedral volume $\langle V \rangle$ which measures the tetrahedron's size growth and $\langle I_2 \rangle$ which measures its shape's change. We first compare our findings with Pumir *et al.*'s [5] who used DNS to study the evolution of tetrahedrons for a relatively moderate Reynolds number $R_\lambda=82$ or $k_N/k_1=185$.

The evolution of $\langle I_2 \rangle$ as a function of tu'/L for $k_N/k_1=185$ and different initial sizes Δ_0/η, namely $\Delta_0=0.25\eta$, η, 4η, 16η, 32η, and 64η is shown in Fig. 19. $\langle I_2 \rangle$ is found to decrease rapidly due to the strong shape distortion of the tetrahedron towards a minimum value. This minimum value is an increasing function of the initial size Δ_0. The maximum shape distortion is observed for $\Delta_0/\eta=0.25$ at $tu'/L \simeq 2$.

At large times, $tu'/L > 15$, all the curves corresponding to different initial sizes approach the asymptotic value

$$\langle I_2 \rangle_\infty = 0.215$$

which corresponds to a Gaussian distribution of $\langle I_2 \rangle$. The exact Gaussian value for a three-dimensional turbulent flow is $\langle I_2 \rangle_{Gau}=0.222$ corresponding to a Gaussian distribution of ρ_1, ρ_2, and ρ_3 [5].

It can also be noticed that as the initial triangle size increases, the shape's distortion becomes smaller. So that when the initial tetrahedron size becomes comparable to the largest length scale L_1 ($\Delta_0 \simeq 0.5L_1$), $\langle I_2 \rangle$ eventually decreases from its initial value to its asymptotic value monotonically without

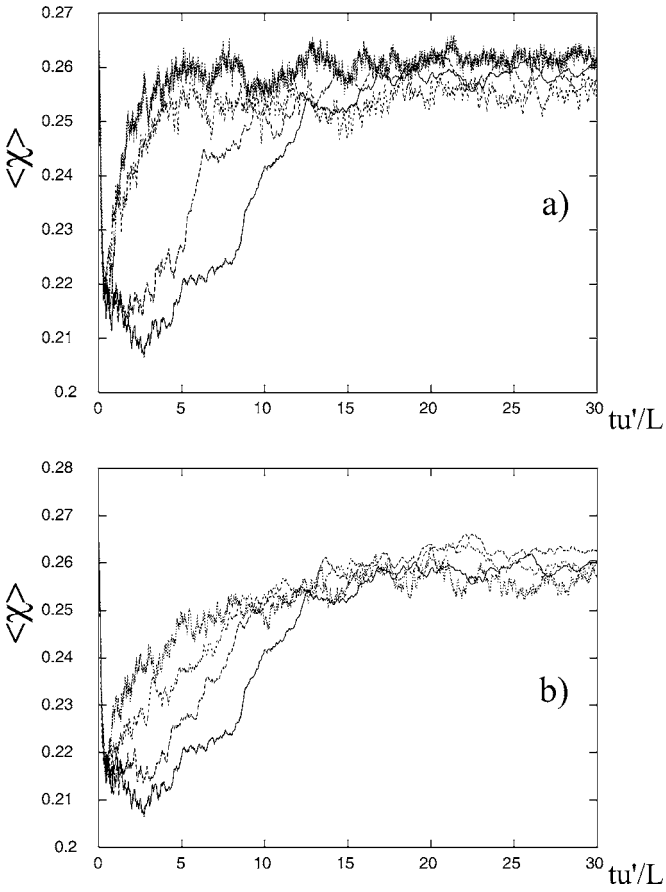

FIG. 16. Time evolution of $\langle\chi\rangle$ for $k_N/k_1=1000$, $\Delta_0/\eta=0.25$, and different unsteadiness parameters $\lambda=0$, 1, 5, and 20 defined by (a) the first method and (b) the second method.

reaching a local minimum, in contrast to what is observed for smaller initial tetrahedron sizes ($\Delta_0 \ll 0.5L_1$). All these results are similar to those observed for a triangle.

Figure 20 shows the evolution of the tetrahedron's volume $\langle V\rangle$ as a function of time for different initial sizes, namely $\Delta_0=0.25\eta$, η, 4η, 16η, 32η, and 64η. At short times, the volume is conserved due to incompressibility. Once inertial

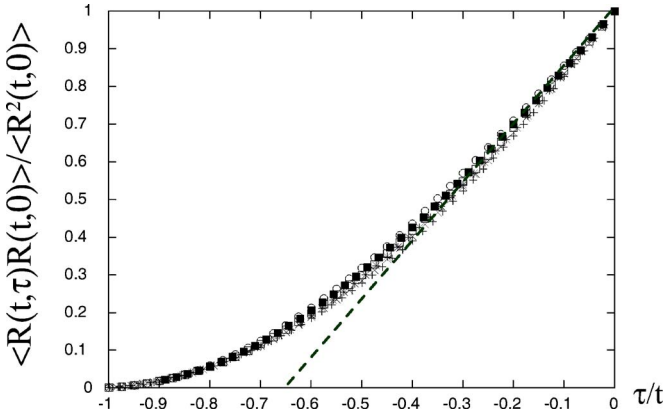

FIG. 17. (Color online) Lagrangian correlation function of the triangle size for $\Delta_0/\eta=0.25$ and different times in Richardson's regime: $tu'/L=2.5$ (+), 3 (×), 3.5 (∗), 4 (□), 4.5 (■), and 5 (○).

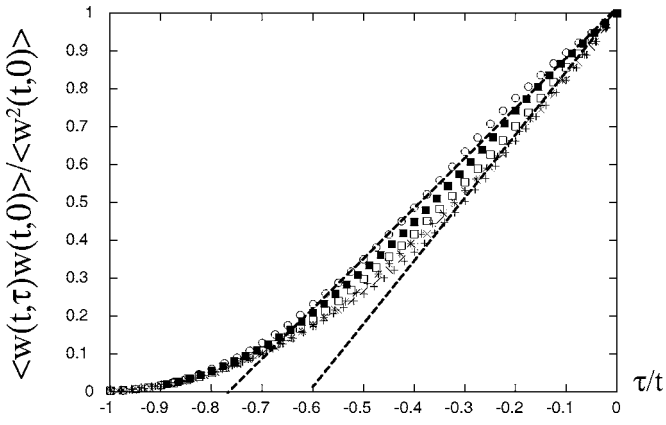

FIG. 18. Lagrangian correlation function of the parameter $\langle w\rangle$ for $\Delta_0/\eta=0.25$ and different times in Richardson's range $tu'/L=2.5$ (+), 3 (×), 3.5 (∗), 4 (□), 4.5 (■), and 5 (○).

scales are reached, the contribution of small-scale fluctuations becomes important enough to affect the dynamics of the tetrahedral volume. The volume deviates from the linear volume-preserving map that it followed in the dissipative range and the average volume begins to increase [5]. In the inertial range, Richardson's scaling $\langle|V|\rangle \sim \epsilon^{3/2}t^{9/2}$ seems to be only valid at $\Delta_0=\eta$ as indicated by the straight line. The volume increase follows that trend until very large times ($tu'/L>10$) when the increase saturates onto a t^3 law as indicated by the dashed straight line. This later regime corresponds to the random walk regime when two particles become independent and their distance becomes proportional to t.

B. Results for larger Reynolds numbers

From the previous results, KSs are found to satisfactorily predict most features of the four-particle diffusion in isotropic three-dimensional turbulence in comparison with the results obtained with DNS from Ref. [5]. So we will now consider larger inertial subranges to show the role of large Reynolds numbers on the four-particle diffusion.

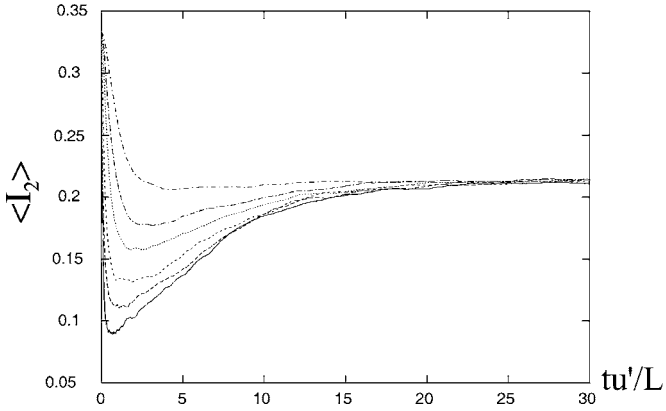

FIG. 19. Evolution of $\langle I_2\rangle$ as a function of tu'/L for $k_N/k_1=185$ and different initial tetrahedron sizes, namely from bottom to top $\Delta_0/\eta=0.25$, 1, 4, 16, 32, and 64.

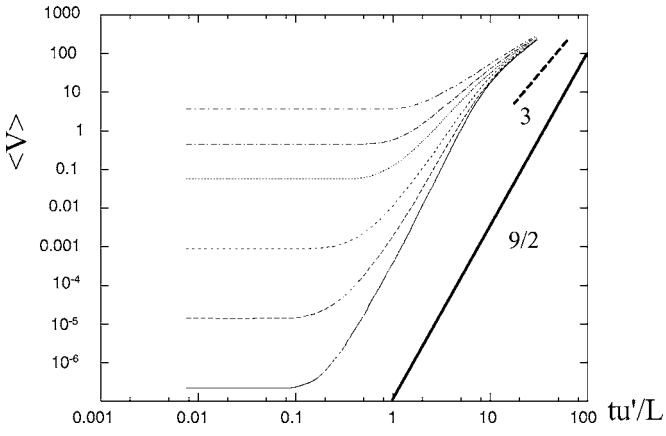

FIG. 20. Evolution of $\langle V \rangle$ as a function of tu'/L for $k_N/k_1=185$ and different initial tetrahedron sizes, namely from bottom to top $\Delta_0/\eta=0.25$, 1, 4, 16, 32, and 64.

Figure 21 shows the evolution of $\langle I_2 \rangle$ as a function of tu'/L for different inertial subranges, $k_N/k_1=185$, 1000, and 2000 and an initial tetrahedron's size $\Delta_0/L_1=0.032$. With Δ_0/L_1 fixed, all the curves collapse for all Reynolds numbers. The same result is observed for $0.032 \leqslant \Delta_0/L_1 \leqslant 0.5$. Figure 22 shows the evolution of $\langle V \rangle$ as a function of tu'/L for the different inertial ranges that were considered in Fig. 21, the figure shows that there is no effect of the Reynolds number on $\langle V \rangle$ for a fixed Δ_0/L_1. Pumir *et al.* concluded that results do not depend qualitatively on the Reynolds number in the range $21<R_\lambda<82$. We can extend this range to a higher limit $k_N/k_1=2000$ which corresponds to $R_\lambda=400$. We can also extend the interpretation we gave for triangles to tetrahedrons: what matters in the building up of $\langle I_2 \rangle$, $\langle w \rangle$, and $\langle V \rangle$ is the scales present inside the volume, that is the ratio L/Δ_0. Their time evolution is controlled by L/Δ_0, that is the range of turbulent scales the initial tetrahedron encompasses, not by the Reynolds number.

Figure 23 shows the evolution of $\langle I_2 \rangle$ as a function of tu'/L for $k_N/k_1=2000$ and for different initial triangle sizes (Δ_0), namely $\Delta_0/\eta=0.25$, 1, 4, 16, 64, and 1000. The dependence of $\langle I_2 \rangle$ on the initial tetrahedron's size is shown to be

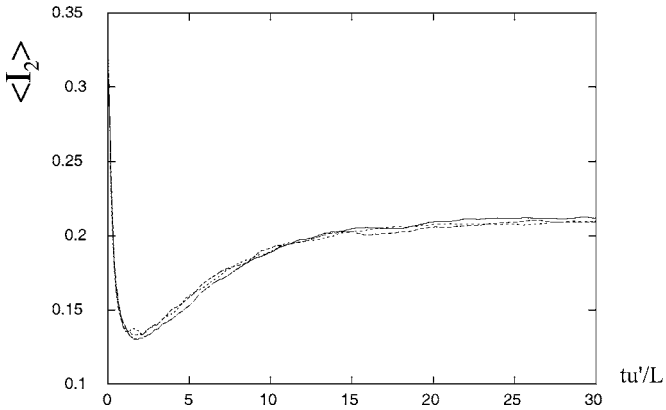

FIG. 21. Evolution of $\langle I_2 \rangle$ as a function of tu'/L at different inertial subranges $k_N/k_1=185$, 1000, and 2000 for tetrahedrons of initial sizes of $\Delta_0/L_1=0.032$.

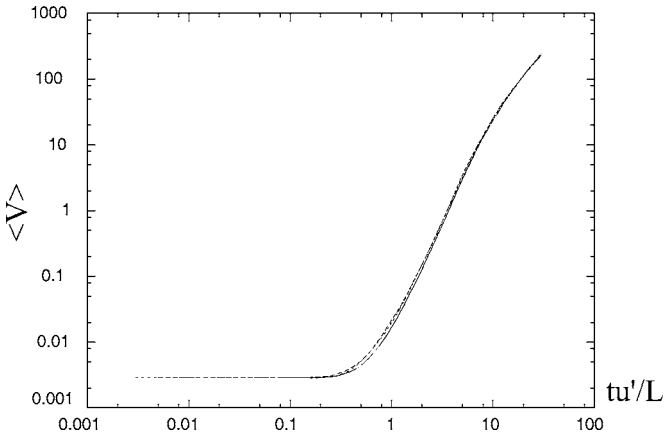

FIG. 22. Evolution of $\langle V \rangle$ as a function of tu'/L at different inertial subranges $k_N/k_1=185$, 1000, and 2000 for small inertial tetrahedron sizes of $\Delta_0/L_1=0.032$.

weaker than the one observed for small Reynolds numbers (Fig. 19). For large times, $\langle I_2 \rangle$ approaches an asymptotic value, which is the Gaussian value. Similarly to what was found for $k_N/k_1=185$, when the initial tetrahedron's size becomes comparable to the largest length scale L_1 (i.e., $\Delta_0 \simeq 0.5L_1$, as seen in the case $\Delta_0=1000\eta$), we find that $\langle I_2 \rangle$ decreases directly from its initial value to its asymptotic value without reaching a local minimum in contrast with what can be seen for triangles of smaller initial sizes $(\Delta_0 \ll 0.5L_1)$. So, we can conclude that if the initial tetrahedron's size is in the inertial range but much larger than the Kolmogorov microscale, the distortion in shape becomes very small. This would be because tetrahedrons with large enough initial sizes may not be affected by the small scale fluctuations of the turbulent field. These results are similar to those found for the triangle and are underlain by the same explanations.

Figure 24 shows the evolution of $\langle V \rangle$ as a function of tu'/L for $k_N/k_1=2000$ and different initial tetrahedron sizes, namely $\Delta_0/\eta=0.25$, 1, 4, 16, 64, and 1000. In this type of representation, Richardson' s scaling seems to be only valid for $\Delta_0=4\eta$.

C. Effect of the unsteadiness term

Figure 25 shows the evolution of $\langle I_2 \rangle$ as a function of tu'/L for $k_N/k_1=1000$, $\Delta_0/\eta=0.25$, and different unsteadi-

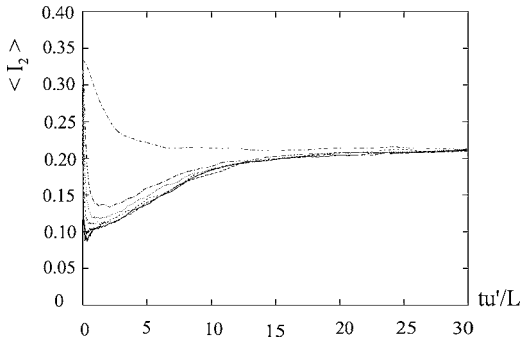

FIG. 23. Evolution of $\langle I_2 \rangle$ as a function of tu'/L for $k_N/k_1=2000$ and for different initial tetrahedron sizes (Δ_0), namely from bottom to top $\Delta_0/\eta=0.25$, 1, 4, 16, 64, and 1000.

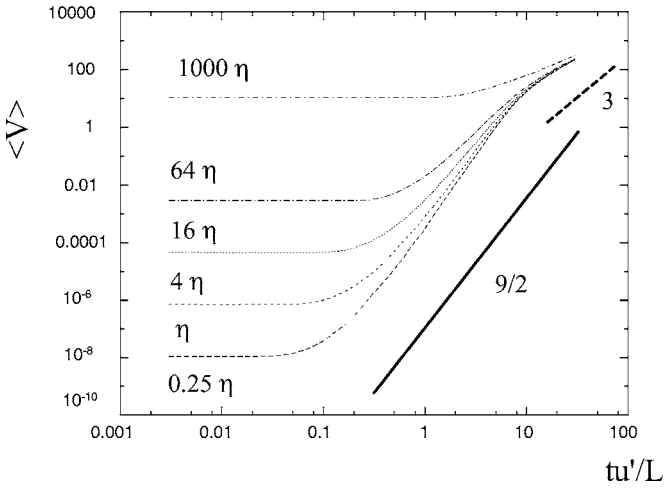

FIG. 24. Evolution of $\langle V\rangle$ as a function of tu'/L for $k_N/k_1=2000$ and for different initial tetrahedron sizes, namely $\Delta_0/\eta=0.25$, 1, 4, 16, 64, and 1000.

ness parameters $\lambda=0$, 1, and 5 defined by the first method (a) and the second method (b). The conclusions are very similar to those drawn for the triangle. With the second method there is less than 10% discrepancy whatever the value for λ. With the first method there is less than 10% discrepancy provided that $\lambda\in[0,1]$. For $0<\lambda<1$ defined by either method the asymptotic value of $\langle I_2\rangle$ is the same as the Gaussian value

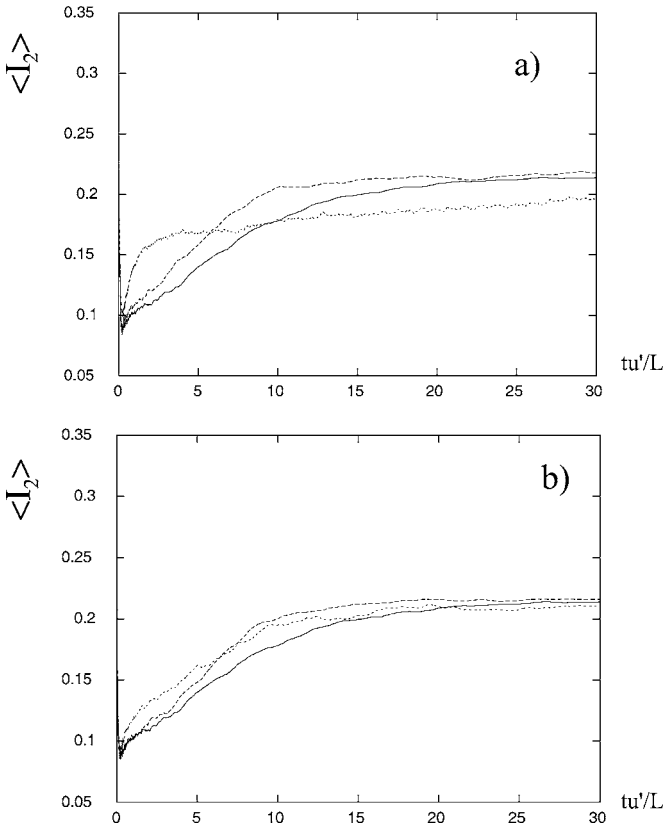

FIG. 25. Evolution of $\langle I_2\rangle$ as a function of tu'/L for $k_N/k_1=1000$, $\Delta_0/\eta=0.25$, and different unsteadiness parameters $\lambda=0$, 1, and 5 defined by the first method (a) and the second method (b).

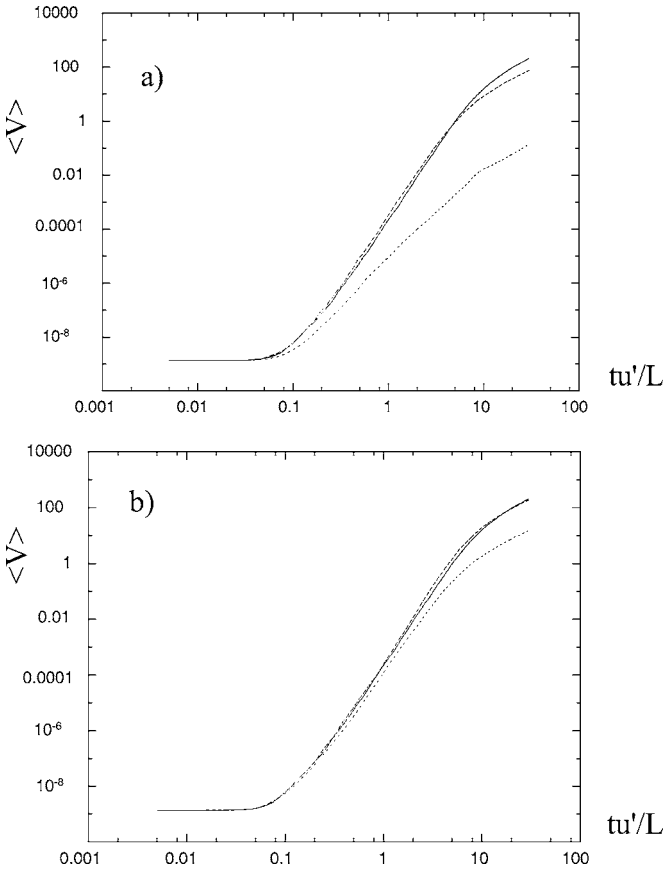

FIG. 26. Evolution of $\langle V\rangle$ as a function of tu'/L for $k_N/k_1=1000$, $\Delta_0/\eta=0.25$, and different unsteadiness parameters $\lambda=0$, 1, and 5 defined by the first method (a) and the second method (b).

($\approx$0.222). When $\lambda=5$ the asymptotic value becomes smaller than its corresponding Gaussian value.

Figure 26 shows the evolution of the tetrahedron's volume $\langle V\rangle$ as a function of tu'/L for $k_N/k_1=1000$, $\Delta_0/\eta=0.25$, and different unsteadiness parameters $\lambda=0$, 1, and 5 defined by the first method (a) and the second method (b). The figure shows that there is no effect of λ on the evolution of the tetrahedral volume when time is less than $7tu'/L$ when the first method is used, and at all times when the second method is used provided that $0<\lambda<1$.

VI. CONCLUSIONS

We studied the evolution of three- and four-particle diffusion at large Reynolds numbers using kinematic simulation in isotropic turbulence. We found that

(i) KS is able to predict the evolution of three- and four-particle diffusion in isotropic turbulent flows. The results obtained are in a very good agreement with those obtained using DNS in Ref. [5] for moderate Reynolds numbers.

(ii) The evolution of the triangle (respectively tetrahedron) depends on whether the value of the triangle size $\langle R^2\rangle^{1/2}$ (respectively tetrahedron volume $\langle V\rangle$) lies in the Richardson range. If it does, there is a nontrivial shape distortion. If $\langle R^2\rangle^{1/2}$ (respectively $\langle V\rangle^{1/3}$) is larger than the largest length scale, then the shape of the triangle (respectively tet-

rahedron) relaxes to an asymptotic value corresponding to a Gaussian distribution of the eigenvalues ρ_i.

(iii) The evolution of $\langle W\rangle$, $\langle \chi\rangle$, $\langle I_2\rangle$ for three and four particles and $\langle V\rangle$ for four particles as a function of $u't/L$ does not depend on the Reynolds number but only on the ratio Δ_0/L_1, that is on the portion of the inertial range that is contained within the initial triangle or tetrahedron. We extend these results discussed in Ref. [5] for small Reynolds numbers to the higher limit $k_N/k_1=2000$ corresponding to $R_\lambda=400$.

(iv) There is no effect of λ when $0\leqslant\lambda\leqslant 1$ on the evolution of the triangle radius of gyration and tetrahedral volume for times less than $7tu'/L$ if λ is defined by the first method, and at any time if λ is defined by the second method. The second method of modeling the unsteadiness parameter seems very robust and has no dependence on λ whenever $\lambda\in[0,1]$.

(v) The evolution of the radius of gyration of the triangle is shown to be self-similar in time. This self-similarity observed on the radius of gyration is not so well observed on the Lagrangian correlation function of the parameter $\langle w\rangle$ describing the geometry change evolution.

ACKNOWLEDGMENTS

F. Nicolleau acknowledges EPSRC sponsorship through Grants No. GR/N22601, No. GR/R64957, and No. GR/S95633/01.

[1] G. K. Batchelor, Proc. R. Soc. London, Ser. A **213**, 349 (1952).
[2] K. R. Sreenivasan, Proc. R. Soc. London, Ser. A **434**, 165 (1991).
[3] L. Mydlarski, A. Pumir, B. I. Shraiman, E. D. Siggia, and Z. Warhaft, Phys. Rev. Lett. **81**, 4373 (1998).
[4] G. Falkovich, K. Gawedzki, and M. Vergassola, Rev. Mod. Phys. **73**, 913 (2001).
[5] A. Pumir, B. I. Shraiman, and M. Chertkov, Phys. Rev. Lett. **85**, 5324 (2000).
[6] B. I. Shraiman and E. D. Siggia, Phys. Rev. E **57**, 2965 (1998).
[7] P. Castiglione and A. Pumir, Phys. Rev. E **64**, 056303 (2001).
[8] F. Nicolleau and J. C. Vassilicos, Phys. Rev. Lett. **90**, 024503 (2003).
[9] P. Flohr and J. C. Vassilicos, J. Fluid Mech. **407**, 315 (2000).
[10] N. A. Malik and J. C. Vassilicos, Phys. Fluids **11**, 1572 (1999).
[11] F. Nicolleau and A. ElMaihy, J. Fluid Mech. **517**, 229 (2004).
[12] M. A. I. Khan, A. Pumir, and J. C. Vassilicos, Phys. Rev. E **68**, 026313 (2003).
[13] A. Pumir, Phys. Rev. E **57**, 2914 (1998).
[14] A. Celani and M. Vergassola, Phys. Rev. Lett. **86**, 424 (2001).
[15] J. C. H. Fung, J. C. R. Hunt, N. A. Malik, and R. J. Perkins, J. Fluid Mech. **236**, 281 (1992).
[16] J. C. Vassilicos and J. C. H. Fung, Phys. Fluids **7**, 1970 (1995).
[17] J. Davila and J. C. Vassilicos, Phys. Rev. Lett. **91**, 144501 (2003).
[18] F. W. Elliott and A. J. Majda, Phys. Fluids **8**, 1052 (1996).
[19] F. Nicolleau and G. Yu, Phys. Fluids **16**, 2309 (2004).
[20] We use the term range rather than regime as we do not intend to discuss here whether or not such a regime is well observed; we refer to Refs. [8,19] for more information on Richardson's regime validity.